PERGAMON

Deep-Sea Research II 50 (2003) 579–603

DEEP-SEA RESEARCH
PART II

www.elsevier.com/locate/dsr2

The effect of marginal ice-edge dynamics on production and export in the Southern Ocean along 170°W

Ken O. Buesseler[a,*], Richard T. Barber[b], Mary-Lynn Dickson[c], Michael R. Hiscock[b], Jefferson Keith Moore[d], Raymond Sambrotto[e]

[a] *Department of Marine Chemistry and Geochemistry, Woods Hole Oceanographic Institution, Woods Hole, MA 02543, USA*
[b] *Duke University Nicholas School of the Environment and Earth Sciences, 135 Duke Marine Lab Road, Beaufort, NC 28516, USA*
[c] *Graduate School of Oceanography, University of Rhode Island, Narragansett, RI, 02882, USA*
[d] *National Center for Atmospheric Research, Boulder, CO 80307, USA*
[e] *Lamont Doherty Earth Observatory of Columbia University, Palisades, NY 10964, USA*

Accepted 15 September 2002

Abstract

We present a synthesis of the rates of gross, new, net and primary production along with particulate organic carbon (POC) flux at 100 m from four cruises along 170°W in the Southern Ocean. Concurrent satellite pigment data, a primary productivity model, and a nitrate mass balance are used to extrapolate daily production estimates in space and time to seasonal and annual rates. From this analysis, we gain a better understanding of the timing, magnitude and impact of the phytoplankton blooms in this region. One of the dominant features with respect to plankton biomass is the association of high chlorophyll levels with the retreat of the sea ice which begins in October just south of the Polar Front. Our primary production model and satellite pigment data suggest higher production and flux levels characterize the marginal ice zone than previous estimates. Elevated rates of new production in ice impacted regions are restricted to relatively short periods following retreat of the ice edge. Export is found to lag the onset of production by up to 1 month. The ratio of POC flux at 100 m to primary production when averaged over the entire season is quite high, increasing from 15% to 25% in the Subantarctic zones to 35–40% near the Polar Front and as high as 50–65% in the southernmost stations, just north of the Ross Sea gyre. Comparisons of phytoplankton community structure and Fe stress indicators suggest that blooms at the Polar Front are initially dominated by large centric diatoms, but are replaced by smaller pennate diatom and non-diatom species as Fe levels decrease. Further south, where Fe levels are never as high and large diatoms are not found, we still observe relatively high biomass and elevated production rates and POC fluxes during the short growing season.

1. Introduction

The Southern Ocean is a region characterized by high concentrations of surface macronutrients and relatively low chlorophyll levels. Enhanced uptake of carbon is thus possible if changes in upper

*Corresponding author. Tel.: +1-508-289-2309; fax: +1-508-457-2193.
E-mail address: kbuesseler@whoi.edu (K.O. Buesseler).

0967-0645/03/$ - see front matter © 2003 Elsevier Science Ltd. All rights reserved.
doi:10.1016/S0967-0645(02)00585-4

ocean biogeochemistry lead to the more efficient utilization of available nutrients. Models suggest that alterations to the Southern Ocean carbon balance have the potential to influence climate through the ocean uptake of dissolved inorganic carbon and the impact this would have on atmospheric CO_2 levels (Sarmiento and Orr, 1991; Joos and Siegenthaler, 1991; Sarmiento and Le Quéré, 1996). Therefore, understanding the relative rates and controls on production and export in the Southern Ocean is of considerable interest. However, variability in seasonal and spatial patterns of chlorophyll levels and particle flux are large, making results from any one site or study difficult to extrapolate into models of the Southern Ocean C cycle. In addition, conditions for sampling in these remote, cold and seasonally ice covered regions are poor and concurrent biogeochemical measurements over a complete annual or seasonal cycle in this region are sparse. This unequal distribution of field data in space and time has been noted in earlier reviews of Southern Ocean biogeochemistry, e.g. Tréguer and Jacques, 1992.

The data summarized here are an attempt to provide a more complete picture of the Southern Ocean C cycle using field data collected over a single spring/summer growth cycle as part of the Antarctic Environment and Southern Ocean Process Study (AESOPS), a component of the US Joint Global Ocean Flux Study (JGOFS). We present biological, geochemical and physical data from four cruises to examine the timing, magnitude and controls on phytoplankton blooms and C fluxes in this region. In addition to these cruise-based data, we take advantage of concurrent satellite estimates of surface chlorophyll concentration, sea surface temperature (SST) and sea ice cover fields to extrapolate along this transect in space and time to regions where there were no ship-based observations.

These data thus allow for a more complete analyses of the major Antarctic subsystems south of New Zealand, including Subantarctic, Polar Frontal and Seasonal Ice Zones (SIZs) as well as the northern Ross Sea system. From the perspective of biogeochemical models, differences in the rates of C uptake and particulate organic carbon (POC) export need to be parameterized for these subsystems. The Polar Frontal Zone (PFZ) is thought to exhibit increased phytoplankton biomass as a result of mesoscale eddies and mixing along the front (e.g. for AESOPS see: Moore et al., 1999; Abbott et al., 2000; Barth et al., 2001). High silica fluxes to the sediments below the PFZ are found to be correlated to the blooms of large diatoms which sink to the deep sea forming the sedimentary opal belt surrounding Antarctica (Demaster et al., 1991; Pondaven et al., 2000). North of the PFZ in the Subantarctic Zone (SAZ), smaller nano- and pico-plankton dominate the phytoplankton biomass (Griffiths et al., 1999; Kopczynska et al., 2001), and shifts to lower export:production ratios might be expected. The SIZ compromises an area equal to that of the Antarctic continent, and the southward progression of melting ice is observed to stabilize the vertical water column due to the influence of low-density meltwater, which may also provide enhanced micronutrients, such as iron, during bloom initiation periods (Smith and Nelson, 1985; Sedwick and DiTullio, 1997). Our goal is to use production and export data to examine the ice melt bloom dynamics, including the timing of the onset of the spring bloom, its progression southward as the season advances and the relative patterns and controls on the export ratio in this region. In the process of comparing the C flux data across different ecological subsystems, we obtain a better constrained budget of C uptake and export than for perhaps any other sector of the Southern Ocean.

2. Sampling and analyses

2.1. Sampling

Samples for rate process measurements were collected on four AESOPS cruises identified here as: Cruise 1, October 20–November 24, 1997 (R/V *Roger Revelle* KIWI-6); Cruise 2, December 2, 1997–January 3, 1998 (KIWI-7); Cruise 3, January 8–February 8, 1998 (KIWI-8); and Cruise 4, February 13–March 19, 1998 (KIWI-9). Not all measurements discussed here were made on all

four cruises, and in general, coverage for productivity rates was confined to Cruises 2 and 4 (known within US JGOFS as "Process cruises" I and II, respectively), while export estimates are available from all four cruises, but with more limited spatial coverage on Cruises 1 and 3 (known as "Survey cruises" I and II, respectively).

The AESOPS data and mean position of frontal features were used to define the boundaries of different biogeochemical regions that occur along the transect at 170°W between 50°S and 72°S. The nomenclature used to define this zonation is: Central Subantarctic Zone (C-SAZ) 50–55°S; North of Antarctic Polar Front (N-APF) 55–59°S; Antarctic Polar Front (APF) 59–61.5°S; South of Antarctic Polar Front (S-APF) 61.5–65.5°S; South of Antarctic Circumpolar Current (S-ACC) 65.5–68°S; North of Ross Sea (N-RS) 68–72°S. The major features of these waters are outlined in Table 1. The four zones used between 55°S and 68°S are identical to those used by Nelson et al. (2002) as well as by other recent AESOPS references (Buesseler et al., 2001; Dickson and Orchardo, 2001), and thus were also chosen here for ease of comparison to other seasonal and annual budgets. Since the seasonal ice advances as far north as 62–64°S, the SIZ includes the S-APF, S-ACC and N-RS latitudinal bands.

Table 1
Summary of major oceanographic characteristics observed in AESOPS during the austral spring and summer

	50–55°S	55–59°S	59–61.5°S	61.5–65.5°S	65.5–68°S	68–72°S
	C-SAZ[a]	N-APF[b]	APF[c]	S-APF[d]	S-ACC[e]	N-RS[f]
Ice (week when average ice cover <50% in spring)	Ice free	Ice free	Some ice in early season at southern edge	24 Oct. 1997	12 Dec. 1997	26 Dec. 1997
Temperature average upper 100 m (°C): min/max	7.0/10.1	4.2/6.7	1.8/4.3	−1.7/3.1	−1.1/0.1	−1.1/0.8
Dichothermal layer (temp. min. <0°C)	No	No	Some stations (early season)	Yes	Yes	Yes
Si average upper 100 m (μmol): max/min	3.0/0.5	9.4/2.9	27.1/4.7	60.0/13.7	65.0/59.7	63.2/57.5
NO_3 average upper 100 m (μmol/l): max/min	17.2/11.1	23.8/20.4	27.2/22.7	30.4/24.3	27.8/25.7	25.8/24.9
Fe average upper 100 m (nmol/l)	0.16	0.16	0.18	0.17	0.13	0.12
Chlorophyll-*a* average upper 100 m (mg/m^3): max	0.81	0.19	0.48	1.4	0.62	0.28
Fucoxanthin average upper 100 m (mg/m^3): max	0.43	0.08	0.27	1.0	0.39	0.12
Depth of 1% light and mixed layer (m) at time of max Chl: 1%/MLZ	35/36	53/84	39/18	27/13	Nd/18	46/33
P^B_{opt} (mg C mg Chl^{-1} h^{-1}) min/max	2.9/5.3	2.7/4.1	2.3/5.8	1.5/5.6	1.7 (Cruise 4)	2.8 (Cruise 4)

[a] 50–55°S: C-SAZ, Central Subantarctic Zone. Relatively low nitrate (11–17 μM) and low silicate (0.5–3 μM).

[b] 55–59°S: N-APF, North of Antarctic Polar Front. Within Antarctic Cirumpolar Current (ACC) but north of APF. High relative nitrate (>20 μM) and low Si (max <10 μM).

[c] 59–61.5°S: APF, Antarctic Polar Front. Maximum meridional gradients in both surface and subsurface temperature and density and maximum zone of eastward velocities. Strong mesoscale variability and gradients in silicate.

[d] 61.5–65.5°S: S-APF, South of Antarctic Polar Front. Strong seasonal ice-melt influence. Highest seasonal drawdown in silicate and highest regional Chlorophyll and diatom pigment maxima.

[e] 65.5–68°S: S-ACC, South of ACC front. Strong seasonal ice-melt influence. High and relatively invariable silicate and low relative Fe.

[f] 68–72°S: N-RS, North Ross Sea, Strong seasonal ice-melt influence. Late season Chlorophyll maximum. High and relatively invariable silicate and low relative Fe.

Data summarized from the US JGOFS data base; Fe from Measures and Vink (2001); Pigments from HPLC analyses.

2.2. Analyses

Our focus here is on the rates of gross, net, new and primary production as well as export at 100 m for POC. Manuscripts are now available that describe the individual methods and results summarized here (Sambrotto and Mace, 2000; Buesseler et al., 2001; Dickson and Orchardo, 2001; Hiscock et al., 2003) and primary data can be found on the web via the US JGOFS Planning and Data Management Office (http://usjogfs.whoi.edu). Thus the analytical protocols are only briefly summarized below, except for new data analyses unique to this manuscript where more details are provided.

2.3. Gross, net, primary and new production

Rates of gross and net O_2 production were measured on cruises 2 and 4 using seawater samples from depths corresponding to 100%, 50%, 25%, 10%, 5% and 1% of surface irradiance (Dickson and Orchardo, 2001). Gross O_2 production was determined by adding ^{18}O labeled water to seawater samples and measuring the amount of photosynthetically produced ^{18}O labeled dissolved O_2 in 24 h incubations (Bender et al., 1987). Net O_2 production was determined from the change in the O_2 concentration in incubated samples (Gaarder and Gran, 1927). Gross and net O_2 production rates were scaled to carbon production using photosynthetic quotients of 1.4 for nitrate assimilation and 1.1 for utilization of regenerated nutrients (Laws, 1991).

Primary productivity was measured using ^{14}C techniques (Hiscock et al., 2003). Samples were collected using a trace metal clean rosette from light depths corresponding to 100%, 50%, 25%, 18%, 10%, 5%, 1%, and 0.1% of surface irradiance. Both in situ and on-deck incubations were conducted over 24 h periods. For photosynthesis vs. irradiance incubations, samples were incubated for 2 h in a temperature-controlled blue-light photosynthetron (Lewis and Smith, 1983).

Measurements of nitrate uptake were made using a $^{15}NO_3$ tracer method on Cruises 2 and 4 (Sambrotto and Mace, 2000). The analysis of the parallel productivity estimates addressed in this paper benefits from the similarity among the productivity techniques. For example, the $^{15}NO_3$ uptake samples were taken from the same sampling rosette and Go-Flo bottles described for the ^{14}C and oxygen-based productivity measurements. The samples were usually taken at the same time and from the same light depths. All productivity samples also shared a common in situ incubation procedure although only about 20% of the nitrate uptake rates were measured in this manner. Most nitrate uptake samples were incubated in on-deck incubators that were separate from those used for the ^{14}C incubations.

2.4. Regional nitrate budgets

A budget of surface water nitrate change was constructed to supplement the ^{15}N nitrate uptake measurements that were limited in most regions to only 2 months of the 4–5 month growing season. The rate of change in local nitrate concentration was estimated by combining all of the nitrate casts in a respective latitude region. These data were used to construct a uniform grid of nitrate concentrations that represented a time series in each region. The observed local change reflects advection and vertical mixing in addition to the net biological uptake of nitrate. However, an approximate estimate of the latter term can be isolated from local change due to the unusual features of the ACC region. For example, while meridional nutrient gradients can be very steep (Brzezinski et al., 2001), zonal gradients are much weaker. Thus, although mesoscale and smaller eddy features will also affect the local nutrient fields (Barth et al., 2001), the net zonal advective flux is generally low. The meridional flux of nutrients due to the northward movement of water from the Antarctic Divergence has been estimated at 0.28 mmol $NO_3\,m^{-2}\,d^{-1}$ through the ACC region (Pondaven et al., 2000). This is far less than the maximum $^{15}NO_3$ uptake rates measured here (8–10 mmol $m^{-2}\,d^{-1}$; Sambrotto and Mace, 2000) and thus biological consumption dominates advective fluxes, at least during peak growth periods.

The daily rate estimates were based on the depth-integrated changes. The integration depth

varied among regions and was selected to extend below the average mixed layers for each region. This deeper depth of integration was designed to encompass the vertical diffusive flux as well as periodic mixed-layer deepenings that were not recorded by the sampling. In each region, the integration depth was based on the depth at which relatively uniform nitrate concentrations with time were observed in the gridded data that were assumed to approximate the winter values for surface waters. From north to south, the integration depths used were 103, 110, 130, 80, 73 and 94 m, in the C-SAZ, N-APF, APF, S-APF, S-ACC and N-RS, respectively. These depths reflect the consistently deeper mixed layers in the N-APF and APF bands.

2.5. Export

The POC flux at 100 m was determined using a thorium-234-based approach as adapted from Buesseler et al. (1992) and discussed in more detail for AESOPS in Cochran et al. (2000) and Buesseler et al. (2001). For AESOPS, the activity of total ^{234}Th (half-life = 24.1 d) was determined at seven sampling depths in the upper 300 m. Lower ^{234}Th:^{238}U activity ratios indicate higher particulate flux, and ratios near 1 indicate negligible sinking flux relative to production and decay. In order to estimate POC flux, the calculated ^{234}Th flux is multiplied by the site-specific ratio of POC/^{234}Th measured at depth on filtered particles (collected here on $>70\,\mu m$ screens). In this manner, the POC flux at 100 m was estimated for 4 stations during Cruise 1, 6 for Cruise 3, and 10 each for Cruises 2 and 4. Details of this ^{234}Th flux calculation, a discussion of the application of steady-state vs. non-steady-state models and the determination of physical transport terms can be found in the original reference. In addition, the original reference provides both POC and biogenic Si fluxes (using the bSi: ^{234}Th ratio on $>70\,\mu m$ particles), and compares these shallow fluxes to other estimates of particulate export in the Southern Ocean.

Given its 24 d half life and our flux model, the POC flux determined using this tracer represents particle settling losses of POC that took place *prior* to our arrival. This flux therefore has a "memory" of days to 3–4 weeks, depending upon the relative magnitude and duration of the flux events. Large, short flux events will leave a significant ^{234}Th deficit that lasts for longer periods, relative to smaller or continuous flux events.

2.6. Satellite products

Weekly satellite estimates of surface chlorophyll concentration, SST, and % sea ice cover were constructed for a transect along 170°W (171–169°W) from 75°S to 50°S. The latitudinal resolution along this transect was ~9 km. Daily Level 3 standard mapped images of chlorophyll concentration from SeaWiFS (Version 3.0) were obtained from the Goddard Space Flight Center Distributed Active Archive Center. Daily SST estimates from the NOAA/NASA Pathfinder Program were obtained from the Jet Propulsion Laboratory Distributed Active Archive Center, and daily sea ice cover estimates (NASA Team Algorithm) from the Special Sensor Microwave Imager were obtained from the National Snow and Ice Data Center Distributed Active Archive Center at the University of Colorado, Boulder. These daily images were averaged over weekly time scales during our study period. Weekly data were then averaged over 1° latitudinal bins. Cloud cover prevents satellite estimation of chlorophyll concentration and SST, but does not affect the sea ice measurement. The heavy cloud cover in this region resulted in very sparse data coverage in the daily SST and chlorophyll images. However, by averaging over weekly time scales and 2° of longitude and 1° latitude, we were able to construct fairly complete transects along 170°W over the study period.

2.7. Primary productivity modeling

Using the weekly binned SeaWiFS chlorophyll data, we modeled the seasonal progression of primary production using a Behrenfeld and Falkowski (1997) type model. The Behrenfeld and Falkowski (1997) model calculates primary production using the following algorithms:

$$PP_{eu} = 0.66125\, P^{B}_{opt\ hr} D_{irr} [E_0^+/(E_0^+ + 4.1)] Z_{eu} C_{opt},$$

where PP_{eu} is integrated primary production (mg C m^{-2} d^{-1}), $P^{B}_{opt\ hr}$ is maximum C fixation rate within the water column (mg C mg Chl^{-1} h^{-1}), D_{irr} is the photoperiod (h d^{-1}), E_0^+ is the daily irradiance just above the sea surface (mol quanta m^{-2}), Z_{eu} is the physical depth receiving 1% of E_0^+ (m), and C_{opt} (mg Chl m^{-3}) is the chlorophyll concentration at P^{B}_{opt}.

In this analysis we used C_{sat} (chlorophyll concentration determined by satellite) rather than C_{opt}. Instead of $P^{B}_{opt\ hr}$, we used $P^{B}_{opt\ day}$ (mmol C mg Chl^{-1} d^{-1}), the highest chlorophyll-normalized productivity rate in a 24-h in situ or on-deck primary productivity incubation. $P^{B}_{opt\ day}$ is effectively $P^{B}_{opt\ hr}$ (mg C mg Chl^{-1} h^{-1})D_{irr} (h d^{-1})/12.01 (g C mol C^{-1}); therefore we used the equation:

$$PP_{eu} = 0.66125 \times 12.01 P^{B}_{opt\ day} [E_0^+/(E_0^+ + 4.1)] Z_{eu} C_{sat}.$$

We determined Z_{eu} using an empirical relationship dependent on chlorophyll, latitude, time of year, and spectral attenuation of irradiance within the water (Morel, 1988). E_0^+ was determined by the Gregg and Carder (1990) clear sky model. We determined the clear sky maximum irradiance value based on time of year and latitude and then multiplied by 0.5 to account for persistent cloud cover. $P^{B}_{opt\ day}$ was measured at 36 locations with 24-hour on-deck incubations. P^{B}_{max} was measured with 2-h photosynthesis vs. irradiance experiments at additional 6 stations. These combined estimates and measurements of $P^{B}_{opt\ day}$ were used to extrapolate $P^{B}_{opt\ day}$ values for the entire growing season within each latitudinal band.

3. Results

The primary results are provided in Table 2, binned by latitude and sorted by date. What are summarized here and in the figures are generally only those AESOPS stations where we have made a ship-based estimate of any one of the following rates: gross production, net production, new production, primary production or export using the methods described above. For many of these primary stations, we depict the data in a single figure showing the relative latitudinal position of each station along 170°W running from 75°S to 50°S (*Y*-axis) vs. time (*X*-axis) from October 1, 1997 to March 26, 1998. Data are represented as a series of bubble plots, with the magnitude of each value indicated by the relative bubble size. The seasonal progression of any individual measurement at a given latitude thus follows a horizontal line, and the progression southward and northward of the ship during a given cruise can be easily visualized.

3.1. Physical and geochemical setting

Shown in each figure is the position of the ice edge, defined by satellite data as the point where there is 50% ice coverage (solid line, Fig. 1). Also shown for comparison in the first panel is the position of the ice edge, using either an 80% or 10% criteria (Fig. 1a). At the start of the first cruise in late October, the ice edge using any of the criteria was found between 62°S and 64°S, just south of the mean position of the APF (APF = 59–61.5°S). In other sectors of the Southern Ocean, the APF is further north and there is typically a much wider expanse of open water south of the APF and north of the maximum extent of the winter ice, a region which is called the permanently open ocean zone (POOZ). One feature of this section along 170°W is the absence of a significant POOZ (Moore and Abbott, 2000). The position of the ice edge shifts only about 2° south between early October and late November, near the end of Cruise 1. The retreat of the ice edge to the south was much faster in the following 2–3 months, reaching as far south as 75°S near the end of December using the 80% coverage criteria, or the end of January using the 50% criteria. Using the 10% criteria the ice never receded further south than 73–74°S in this region, and by the time of our fourth cruise in February, the ice edge was progressing to the north, reaching 70–71°S by the end of our observation period.

If we define the SIZ as that region which has at least 5% ice cover during the maximum ice period in August and $<70\%$ in February during the maximum ice free period, than all of our stations south of the APF along 170°W are in the SIZ. The

Table 2
Summary of production and export rates from AESOPS 170°W cruises

Cruise	Station ID	Date (1997–1998)	Latitude (nominal °S)	Gross production (mmol C m^{-2} d^{-1})	Net production (mmol C m^{-2} d^{-1})	Primary production (mmol C m^{-2} d^{-1})	New production (mmol C m^{-2} d^{-1})	POC flux at 100 m (mmol C m^{-2} d^{-1})
50–55°S	C-SAZ							
Cruise 2	1	04-Dec	53.0	398	290	141	84	11
Cruise 2	18	27-Dec	54.3	116	65	78	27	
Cruise 2	19	29-Dec	53.0	112	40	44	14	
Cruise 4	1	15-Feb	53.0	216	68	58	16	13
Cruise 4	29	13-Mar	54.3	71	−11	19	8	5
55–59°S	N-APF							
Cruise 1	1	23-Oct	57.0					15
Cruise 2	2	06-Dec	56.8	97	−18	32	12	5
Cruise 2	17	25-Dec	55.7	105	47	56	13	5
Cruise 4	2	17-Feb	56.9	204	13	29	12	16
Cruise 4	3	19-Feb	58.5			20		
Cruise 4	27	12-Mar	58.5			19		
Cruise 4	28	12-Mar	56.9			16		
59–61.5°S	APF							
Cruise 1	8	31-Oct	60.5			31		15
Cruise 1	12	03-Nov	59.3			23		11
Cruise 1	18	12-Nov	60.2			33		
Cruise 1	23	17-Nov	60.8			50		
Cruise 2	4	08-Dec	60.2			66		
Cruise 2	4	10-Dec	60.2	114	61	65	25	9
Cruise 2	5	11-Dec	60.9	131	39	42	59	19
Cruise 3	6	24-Jan	62.0					11
Cruise 4	4	20-Feb	60.2	40	−20	20	7	12
Cruise 4	5	22-Feb	60.9			20		
Cruise 4	26	11-Mar	60.2			16		
61.5–65.5°S	S-APF							
Cruise 1	3	27-Oct	62.4			19		16
Cruise 2	6	13-Dec	61.7	172	71	64	53	9
Cruise 2	7	16-Dec	64.2	243	151	89	73	6
Cruise 2	8	17-Dec	64.7	270	134	66	44	16
Cruise 2	9	18-Dec	63.1	109	65	76	30	13
Cruise 2	10	21-Dec	62.4	106	66	64	20	
Cruise 3	4	17-Jan	64.8					31
Cruise 3	5	19-Jan	62.0					22
Cruise 3	8	27-Jan	65.2					36
Cruise 4	6	22-Feb	61.7			17		
Cruise 4	7	23-Feb	63.1	42	−1	17	5	18
Cruise 4	8	25-Feb	64.7			20	8	
Cruise 4	18	07-Mar	64.7		2	13	5	15
Cruise 4	19	08-Mar	63.1			12		
Cruise 4	20	09-Mar	61.7	23	2	14	13	4
65.5–68°S	S-ACC							
Cruise 3	3	16-Jan	67.8					16
Cruise 4	9	26-Feb	66.1	58	−6	12		20

Table 2 (*continued*)

Cruise	Station ID	Date (1997–1998)	Latitude (nominal °S)	Gross production (mmol C m^{-2} d^{-1})	Net production (mmol C m^{-2} d^{-1})	Primary production (mmol C m^{-2} d^{-1})	New production (mmol C m^{-2} d^{-1})	POC flux at 100 m (mmol C m^{-2} d^{-1})
Cruise 4	17	06-Mar	66.1			12	10	
Cruise 4	16	06-Mar	67.5			15	10	
68–72°S	N-RS							
Cruise 4	12	28-Feb	69.3			18	8	
Cruise 4	13	01-Mar	70.4			19		
Cruise 4	13	02-Mar	70.4	82	4	16	8	38
Cruise 4	14	03-Mar	71.3			20	9	
Cruise 4	15	04-Mar	69.3	51	−7	17	10	49

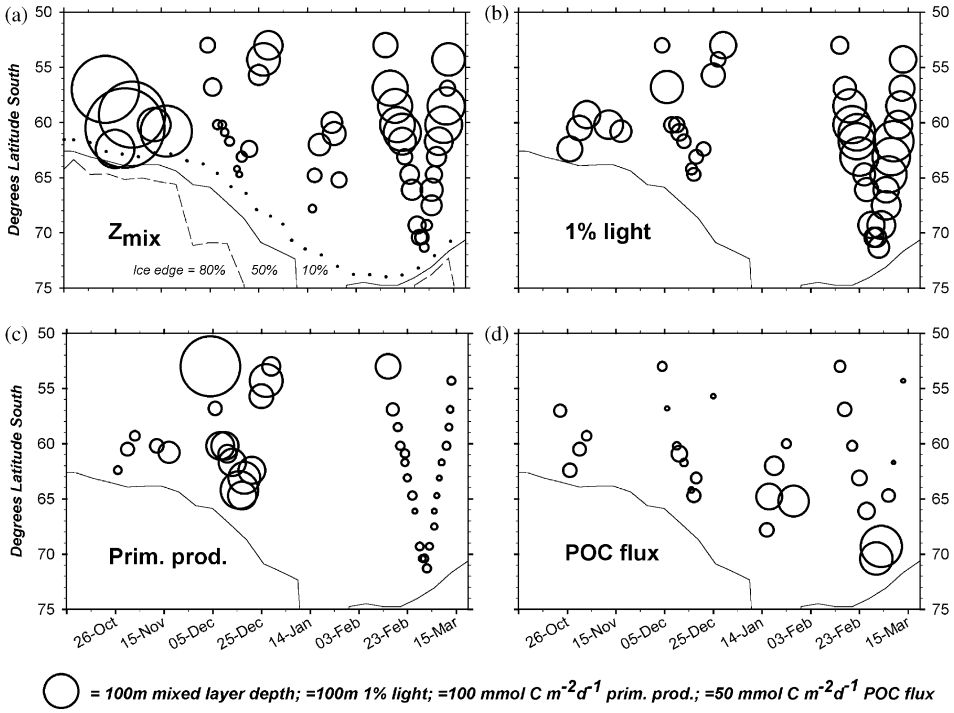

Fig. 1. (a)–(d) Plots showing the time course along 170°W of: (a) mixed-layer depth (in meters, using 0.02 db criteria); (b) depth of 1% light level (in meters); (c). primary (^{14}C) productivity (mmol C m^{-2} d^{-1}); and (d) POC flux derived from ^{234}Th at 100 m (mmol C m^{-2} d^{-1}). Diameter of each circle corresponds to magnitude of each parameter as shown in scale bar along bottom, and the location of each circle indicates position vs. latitude and time as shown along *X* and *Y*-axis. The position of the ice edge as defined by 50% ice cover is shown as a solid line in all panels, while the position of the ice edge as defined by 80% (dashed line) and 10% (dotted line) ice cover is only shown in (a). (e)–(f) Plots showing the time course along 170°W of: (e) gross production (mmol C m^{-2} d^{-1}); (f) new production (mmol C m^{-2} d^{-1}); (g) chlorophyll-*a* (surface 20 m average in mg m^{-3}); and (h) fucoxanthin (mg m^{-3}). Data are plotted as in (a)–(d) with a scale bar along the bottom for the four parameters depicted here.

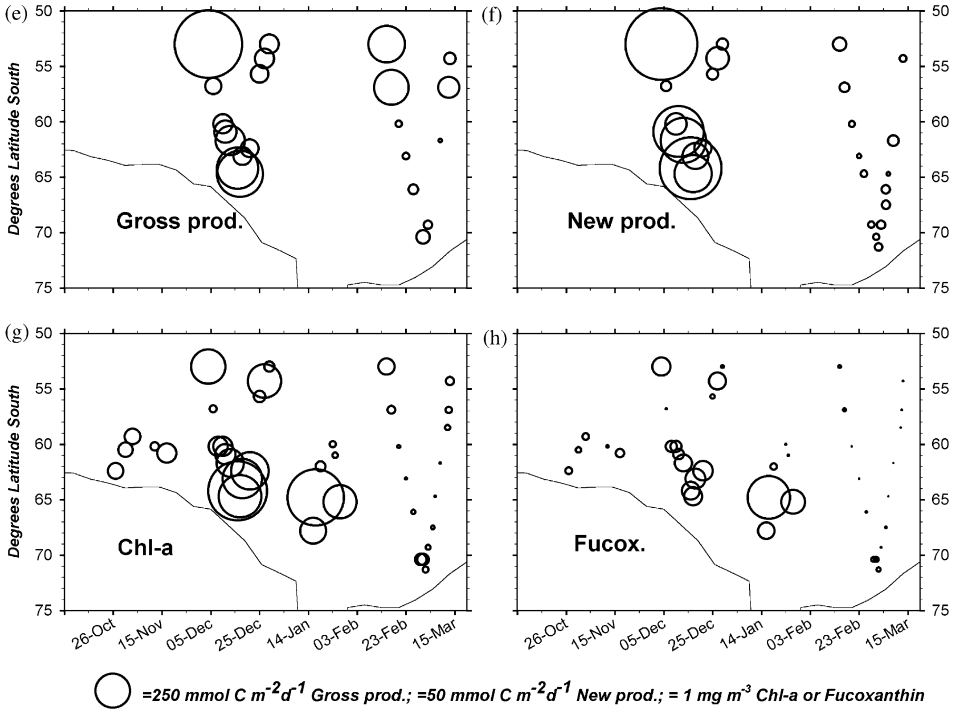

Fig. 1 (*continued*).

marginal ice zone (MIZ) is a subset of the SIZ, defined by recent ice melt within the past month (Smith and Nelson, 1985) and is thought to represent a significantly different ecological zone. Satellite date indicates the MIZ has much higher chlrophyll concentrations than the SIZ as a whole (Moore and Abbott, 2000). Along 170°W, the MIZ moves from 63°S to 70°S as the season progresses.

The mixed-layer depth (Z_{mix}) was quite deep at all stations sampled during October/November time period, ranging from 90 to over 180 m (Z_{mix} defined here using a 0.02 db density difference criteria). At these stations, there was no clear trend vs. latitude in the Z_{mix} however, by the end of Cruise 1 there was some evidence of shoaling mixed layers. By the time of Cruise 2, shallower mixed layers were found at all stations. This is especially prevalent in the region of the APF and southward in the MIZ where within a period of just over 1 month, mixed layers shoaled from >100 to <20 m. This change was due to enhanced stratification as a result of lower surface salinities caused by the melt waters and warming of the surface waters from less than 1°C to 3°C in the MIZ. By the third cruise in January, mixed layers along the APF and S-APF increased again to around 50 m, with a shallower Z_{mix} found associated with recently ice free waters near 68°S. In the late summer on Cruise 4, we see a small deepening of the Z_{mix} at all stations at a given latitude, however generally shallower Z_{mix}'s were still found at the southernmost sites >70°S which were reached for the first time ($Z_{mix} = 20-50$ m). This onset of stratification in the spring and southern progression of shoaling mixed layers, sets the stage for the onset of the spring bloom by the time of our second cruise in December and later in the season at stations within the MIZ. The depth of the 1% light level was shallower than Z_{mix} during Cruise 1, and always greater than Z_{mix} in the three latter cruises at all stations, indicating that light alone would have limited growth during Cruise 1.

The Southern Ocean in general and the AESOPS transect in particular, is characterized by elevated macronutrient levels. Peak nitrate concentrations near 30 μmol l^{-1} were found at all sites from the APF to the southernmost stations at the start of the season. These concentrations decreased only slightly to the north and into the C-SAZ (Table 1). While there was a seasonal drawdown of nitrate at all latitudes, within the N-APF and south thereof, mean nitrate levels in the upper 100 m never dropped below 20 μmol l^{-1}.

Silicic acid on the other hand shows a much stronger latitudinal gradient for both initial concentrations and in the pattern of its seasonal drawdown. Si concentrations were 3 μmol l^{-1} or less in the C-SAZ, and drop from 10 to <3 μmol l^{-1} in the upper 100 m in the N-APF (Table 1). In the APF and south thereof, Si levels of greater than 60 μmol l^{-1} were found. The boundary between these high- and low-Si waters, the Si front, shifted from near 61°S during Cruise 1, to 64°S during Cruise 2 and 65°S during Cruises 3 and 4 (Morrison et al., 2001). At these latitudes, the seasonal pattern of Si uptake associated with diatom blooms is thought to be responsible for the southward migration of the Si front (Franck et al., 2000; Brzezinski et al., 2001). This region of highest Si drawdown also corresponds to the region of highest particulate Si export in both shallow and deep waters, and the location of maximum opal accumulation in the underlying sediments (Honjo et al., 2000; Buesseler et al., 2001; Sayles et al., 2001). South of 65°S, Si remains near 60 μmol l^{-1} throughout the year.

3.2. Production and phytoplankton pigments

Levels of chlorophyll-*a*, primary production and gross, net and new production all show broadly similar patterns during our 5-month observation period (Fig. 1). Productivity rates and pigment levels are all low during Cruise 1 where we encountered the deepest mixed layers. By the start of Cruise 2 in December, we observed elevated production rates and pigment levels in the northernmost stations. In addition, higher rates of production and the highest chlorophyll levels were found to be increasing from the APF to the S-APF in the MIZ. During December, large centric diatoms were abundant in the silica rich waters in this region (Landry et al., 2002). While this diatom-dominated bloom was thus an obvious feature at this time in the cruise data, on a global scale, chlorophyll-*a* levels are never high in this region, reaching only 1–2 mg m^{-3} in the peak bloom periods (Moore et al., 1999; Moore and Abbott, 2000).

There were no productivity measurements made during Cruise 3, but chlorophyll-*a* levels >1 mg m^{-3} were shifted southwards to 65°S, with a significant decrease in the APF region. There were larger relative gradients in fucoxanthin pigments during this time period, when we observed the highest levels of fucoxanthin, a biomarker for diatoms, centered around 65°S (Fig. 1h).

A dramatic decrease in production rates and pigment levels was observed by the time of the late summer Cruise 4. The only stations with moderately elevated production or chlorophyll-*a* levels were in the C-SAZ. In particular, all stations around the APF and as far south as 72°S had extremely low rates of primary production (<20 mmol C m^{-2} d^{-1}) and rates of net production near zero or negative (net heterotrophy; Table 2). There was a small elevation in pigment levels and gross production rates at the southernmost stations near 72°S, but these levels were still lower than those observed at the ice edge at the beginning of the growing season.

3.3. Particulate export

Export shows a similar, but delayed seasonal pattern relative to productivity (compare Figs. 1c and d). There was no indication of high POC fluxes associated with the high productivity and chlorophyll levels in the SAZ during Cruise 2. POC fluxes were found to increase on average between Cruise 2 and Cruise 3, and were highest on the final cruise at our southernmost stations. During this February–March time period, POC fluxes were high at most stations, decreasing only on the northbound transect at 62°S and 54°S near the end of the cruise. Part of this offset in space and time may be due to the different

time scales of production measurements (12–24 h bottle incubations) and calculated export (24 d half-life in situ tracer). The inherent cycle of bloom initiation and collapse is expected to include a rapid increase in the rates of production in response to improved growth conditions in the spring. This would be followed later in the season by export, which could be driven by either limitations related to macro or micronutrient availability, environmental stress (light/temperature) or grazing pressures (see Timing of export vs. production).

3.4. Satellite-derived chlorophyll and sea surface temperature

The satellite-derived chlorophyll and SST data are shown on a similar latitude vs. time scale as the cruise data (Figs. 2a and 2b). Sea ice cover greater than 50% is shown as gray in Fig. 2 and areas in black had no SST or chlorophyll data due to persistent cloud or ice cover. The seasonal evolution in chlorophyll biomass and primary productivity from ship-based measurements can be directly compared to the weekly averaged pigment data (Figs. 1g and 2a). It is clear from these satellite data that the entire 170°W transect had chlorophyll levels $<0.2\,\mathrm{mg\,m^{-3}}$ throughout the October/November timeframe in the early spring. Increased pigments are seen further north in December in the C-SAZ, as corroborated by enhanced production and ship-based chlorophyll levels measured on Cruise 2. At the APF and southward, we see peak chlorophyll levels in the MIZ. This ice-edge bloom follows the retreating ice during Survey II, when there were no productivity estimates but enhanced chlorophyll was observed by the ship south in the MIZ near 65°S. The relatively high chlorophyll levels seen in the satellite data near 68–72°S were not sampled on any of the cruises. By the time of cruise 4, chlorophyll had dropped greatly throughout the region (as seen in both productivity and ship-based pigment data). The only exception is one small bloom at the northern edge of the transect that was not well sampled by the ship.

Satellite SST data, in general, confirm that the waters closest to the retreating ice edge are the coldest, and that this boundary moves south as the season progresses and north again in February (Fig. 2b). There is about a 7–10°C temperature gradient in the surface waters between

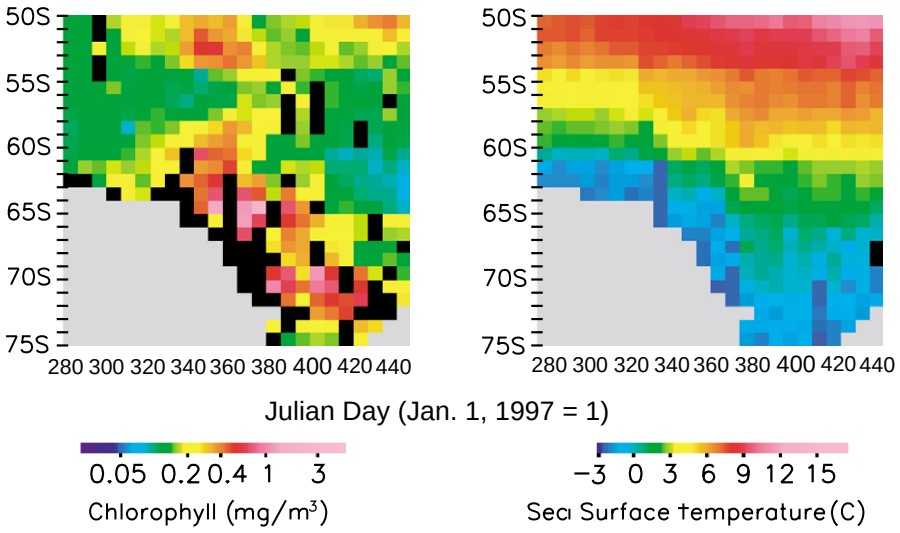

Fig. 2. (a)–(b). Satellite-derived images of surface chlorophyll ($\mathrm{mg\,m^{-3}}$; (a) left) and SST (°C; (b), right). Data are plotted as weekly averages along 170°W, using 2° longitude and 1° latitude binned data. Extent of 50% sea ice cover is shown by gray shaded region and areas in black have no chlorophyll or SST observations during that week.

these colder MIZ waters and the more northerly SAZ.

4. Discussion

4.1. Seasonal dynamics of the ice melt blooms

The most complete record of the temporal and spatial extent of plankton blooms along 170°W is seen in the southward progression of the satellite-derived chlorophyll-*a* peak as blooms develop in the MIZ between December and February (Fig. 2a). Separated further north from this bloom is a chlorophyll maximum in the SAZ in December, with a hint of a smaller bloom at the same latitude in February. In order to compare these data to the ship-based observations, we have plotted the weekly average pigment data vs. time, binned into each of our latitudinal bands (Fig. 3). The standard deviation of the satellite data for any given weekly chlorophyll average is shown by a vertical bar, and in general, we see more variability in satellite-derived chlorophyll during periods of higher biomass. Ship-based measurements of surface chlorophyll (HPLC pigment data from bottle samples within the top 20 m) are shown for comparison, and these data agree quite well with the satellite-derived chlorophyll product. Since these bottle data are single points in space and time and the satellite data are averages of 1 week and binned over a wider latitudinal band, we do not expect an exact correspondence between both data sets. The agreement between the satellite and ship-based chlorophyll data is similar to the conclusion reached by Moore et al. (1999) who found good agreement during AESOPS between SeaWiFS data collected within 24 hours of co-located shipboard measurements ($r^2 = 0.72$; Fig. 3 in Moore et al., 1999). Abbott et al. (2000) also compared SeaWiFS with mooring-derived chlorophyll and found good agreement.

These binned data also show that the chlorophyll maximum occurs within 2–3 weeks of the retreat of the sea ice and that this MIZ bloom moves southward as the season progresses. What is also evident is that the AESOPS cruises did not occupy the southernmost regions during the peak bloom periods in the MIZ, rather the ship arrived somewhat later and thus at low relative biomass levels at latitudes $>65°$S. This has important implications for estimating seasonal and annual productivity balances for the AESOPS study area from the shipboard data alone.

4.2. Modeled primary productivity

We used our modified algorithm to calculate depth-integrated ^{14}C primary production from the SeaWiFS chlorophyll fields. In our modification of the Behrenfeld and Falkowski (1997) primary production model, the notable difference is the treatment of the P^{B}_{opt} variable. Behrenfeld and Falkowski (1997) use a temperature-dependent $P^{B}_{opt\ hr}$ model, while we use a regionally and seasonally dependent extrapolation of measured $P^{B}_{opt\ day}$ values. On average, our estimation of $P^{B}_{opt\ day}$, when converted to $P^{B}_{opt\ hr}$, was 48% higher than the Behrenfeld and Falkowski estimate.

We see a tight correspondence between the modeled weekly primary productivity rates and those measured on the three research cruises (Fig. 4). Primary productivity rates are relatively constant over the course of the season north of the APF, ranging from just under 25–70 mmol C m^{-2} d^{-1}. The highest values are seen during the spring in the APF and later in the season in the waters of the MIZ, with values peaking at 150 mmol C m^{-2} d^{-1}. These high productivity rates are a major finding of our analyses of both the ship and satellite-derived results. The ship-based sampling alone was not sufficient to sample the peak biomass and productivity periods as seen in the satellite data. Thus seasonal or annual averages calculated based upon integration of the ship data alone, would provide an underestimate of productivity rates for this region.

Averaging over the entire Southern Ocean, Moore and Abbott (2000) estimated peak production rates for the MIZ during January of 28 mmol C m^{-2} d^{-1}. This includes all areas of the Southern Ocean including many MIZ regions which did not have blooms (Moore and Abbott, 2000). Still, this is well below the peak MIZ productivities in this study. Moore and Abbott (2000) suggested

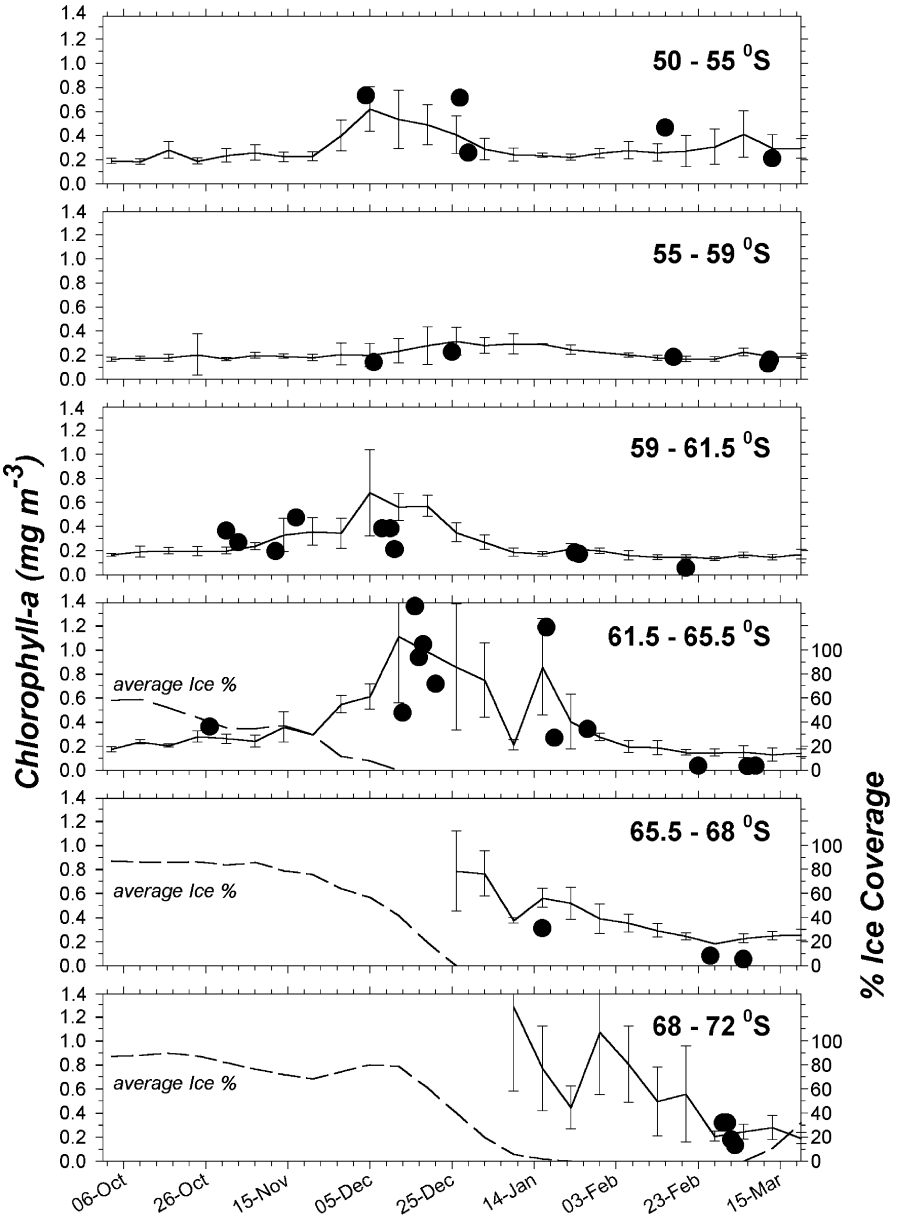

Fig. 3. Plots of surface chlorophyll-*a* (mg m^{-3}; left *Y*-axis) vs. time binned by latitudinal bands as indicated. Ship-based measurements of chlorophyll are shown as solid circles based upon bottle samples. Satellite estimates are averaged over the same latitude bands, and the weekly mean is shown as the solid line, with the standard deviation shown by the vertical bar. Dashed line represents mean ice coverage for a given latitude band corresponding to right *Y*-axis which indicates percent ice coverage as determined by satellites and binned similar to the other data.

that the temperature relation of Behrenfeld and Falkowski (1997) underestimated P^{B}_{opt} and thus productivity in the coldest Antarctic waters. The direct comparion between predicted and measured P^{B}_{opt} values in this study confirms this hypothesis.

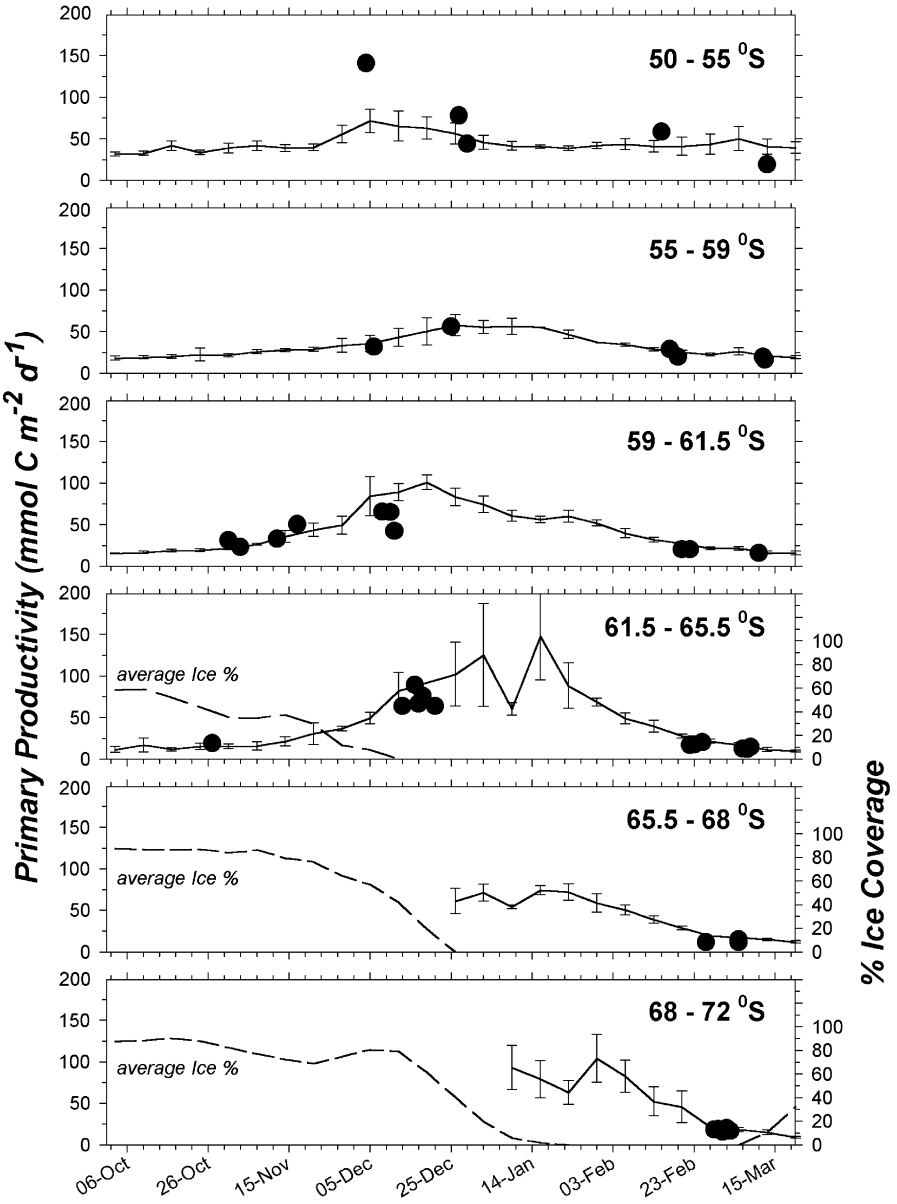

Fig. 4. Plots of primary (^{14}C) production (mmol C m^{-2} d^{-1}; left *Y*-axis) vs. time binned by latitudinal bands as indicated. Ship-based measurements of primary production are shown as solid circles based upon bottle samples. Model estimates are averaged over the same latitude bands, and the weekly mean is shown as the solid line, with the standard deviation shown by the vertical bar. Dashed line represents mean ice coverage as in Fig. 3.

4.3. Seasonal and annual productivity and export rates

Using our modeled primary productivity rates, we now have a more robust method to extrapolate to a seasonal or annual C budget, in that we are not biased by the lack of ship-based measurements during some of the peak biomass periods in the MIZ. For primary productivity, we can simply integrate under the model curve to derive daily

Table 3
Daily average, seasonal and annual organic carbon fluxes

		C flux	C-SAZ 50–55°S	N-APF 55–59°S	APF 59–61.5°S	S-APF 61.5–65.5°S	S-ACC 65.5–68°S	N-RS 68–72°S
Gross production (^{18}O)	Daily average	mmol $m^{-2} d^{-1}$	129.4	120.0	87.4	71.4	57.4	58.4
	Seasonal total	mol m^{-2}	28.1	26.0	19.0	15.5	12.5	12.7
	Annual total	mol $m^{-2} yr^{-1}$	39.6	35.5	22.9	17.6	12.5	12.7
Net production (ΔO_2)	Daily average	mmol $m^{-2} d^{-1}$	60.4	7.9	26.7	48.9	13.8	14.3
	Seasonal total	mol m^{-2}	13.1	1.7	5.8	10.6	3.0	3.1
	Annual total	mol $m^{-2} yr^{-1}$	17.2	1.3	6.1	11.9	3.0	3.1
Primary production (^{14}C)	Daily average	mmol $m^{-2} d^{-1}$	42.8	30.2	36.4	38.5	19.2	19.3
	Seasonal total	mol m^{-2}	9.3	6.5	7.9	8.4	4.2	4.2
	Annual total	mol $m^{-2} yr^{-1}$	13.0	8.7	9.7	9.5	4.2	4.2
New production (^{15}N)	Daily average	mmol $m^{-2} d^{-1}$	24.4	14.8	25.0	15.4	11.9	No est
	Seasonal total	mol m^{-2}	5.4	3.3	5.5	3.4	2.6	No est
	Annual total	mol $m^{-2} yr^{-1}$	5.8	3.7	5.8	3.6	2.7	No est
POC flux at 100 m (^{234}Th)	Daily average	mmol $m^{-2} d^{-1}$	6.8	8.1	13.7	13.9	12.3	10.1
	Seasonal total	mol m^{-2}	1.5	1.8	3.0	3.0	2.7	2.2
	Annual total	mol $m^{-2} yr^{-1}$	2.0	2.4	3.9	4.0	2.7	2.2
POC flux/ primary production (%)			16	27	38	36	64	52

Daily average and seasonal fluxes derived for ice free days between October 7 and May 9th using primary production model as described in the text.
POC flux/primary production ratios calculated from seasonal totals.

average, seasonal integrals and annual rates for primary production in each latitude band. Our satellite data shown in Fig. 2 can be extended to examine a 220 d record from October 1 to May 9 covering the seasonal growth cycle. To calculate an annual rate, we use an average of the low production rates at the start and end of our record to extrapolate to the remaining 145 d at latitudes that are ice free. The under-ice (>50% ice coverage) productivity rates are assumed to be zero. In general, productivity during these 145 d is small, e.g. only 13–23% of the annual totals, for the S-APF and APF, respectively (Table 3). Our assumption of zero production under ice, would tend to underestimate productivity, however progression from 50% to full ice cover takes place quite rapidly and primary production during these early and late season periods is small in any case. One could also argue that offsetting any small underestimate of under-ice productivity is our overestimate of the winter rates, since surface irradiance during the winter months is lower than found in the beginning of October and May, the rates which are used here to calculate the winter average.

During October–May, average daily primary production rates range from 30 to 40 mmol C $m^{-2} d^{-1}$north of 65.5°S and decrease to 20 mmol C $m^{-2} d^{-1}$ further south (Table 3). As an integral over this time period, waters just south of the APF have the highest seasonal primary production levels (8.4 mol C m^{-2}). When these seasonal fluxes are extrapolated to the annual cycle, we find essentially equally high annual primary production

rates of 9.6 mol $m^{-2} yr^{-1}$ in the APF and S-APF regions (Table 3). Nelson et al. (2002) using these same ship-based productivity data and our four latitude bands between 55°S and 68°S, calculated annual average production rates that were 10–20% lower. The major difference can be attributed to our use of a primary productivity model, which includes elevated biomass periods not sampled by the ship

Wefer and Fischer (1991) estimated annual productivity for the PFZ to be 6.9 mol C $m^{-2} yr^{-1}$ and for the combined POOZ and SIZ regions to be only 1.8 mol $m^{-2} yr^{-1}$ based on sediment trap data in the Atlantic sector. Moore and Abbott (2000) estimated mean productivity for the Polar Frontal Region and SIZ for the entire Southern Ocean to be 6.1 and 2.4 mol $m^{-2} yr^{-1}$, respectively. These are significantly lower than our estimates for the AESOPS region along 170°W. The AESOPS region is an area of frequent phytoplankton blooms in both the APF and SIZ, with chlorophyll concentrations and productivity considerably higher than other areas of the Southern Ocean (Moore et al., 1999; Moore and Abbott, 2000). This likely accounts for some of the difference. As mentioned earlier, P^{B}_{opt} in colder waters was also likely underestimated by Moore and Abbott (2000).

Moore and Abbott (2000) estimated a mean productivity in subantarctic waters of 13.3 mol C $m^{-2} yr^{-1}$ in good agreement with our estimate for the C-SAZ (Table 3), but higher than our value of 8.7 mol C $m^{-2} yr^{-1}$ for the N-APF, a region included in the subantarctic average of Moore and Abbott (2000). Nelson et al. (1996) estimated an area weighted average annual production for the nearby Ross Sea shelf region of 11.8 mol C $m^{-2} yr^{-1}$. This is 2–3 times higher than our N-RS and S-ACC regions, but Nelson's average includes the more productive SW Ross Sea shelf which is ice free for longer periods and where chlorophyll values are much higher. A better assessment would be a direct comparison with only the northern Ross Sea data in Nelson et al. (1996). These researchers measured peak primary productivity rates of 80 mmol C $m^{-2} d^{-1}$ at stations along 72.5°S during January–February, similar to our predicted productivities for the 68–72°S region for the same time of year (see Fig. 4).

The annual rates of new production can be analyzed looking at both the regional nitrate budgets and ^{15}N data. Both the rates of nitrate change and the $^{15}NO_3$-based estimates of new production show enhanced N uptake in the APF and S-APF region and along with the retreating ice edge (Fig. 5). The good agreement between the nitrate consumption rates estimated from nitrate budgets and the $^{15}NO_3$ measurements during the spring growing season lends confidence to this approach, especially considering that the $^{15}NO_3$ data are a short-term rate measurement. However, this agreement falls apart during cruise 4, as the entrainment of nitrate from the deepening of the surface mixed layer overwhelmed the biological consumption and produced negative local change estimates (e.g. data from Cruise 4 in late February/early March in Fig. 5). Thus to make an estimate of the seasonal and annual new production rates from nitrate budgets, we used the $^{15}NO_3$ measurements for the late summer period rather than the observed nitrate change at that time. As with the other seasonal production estimates, the satellite data and primary productivity model were used to determine the shape of the nitrate uptake time series in October and November, during periods that were not well sampled. The nitrate uptake values determined in this manner are presented in Table 3.

This seasonal new production estimate from the nitrate balance for the S-APF is similar to that made by Sambrotto and Mace (2000). However, our values for the N-APF and APF regions are over 40% greater than these earlier estimates. These regions were sparsely sampled by the ^{15}N incubation methods and the local nitrate balance in these cases likely provides a more reliable basis for seasonal extrapolations.

For gross and net production and POC export rates, we have used the same seasonal pattern from our primary productivity model, to extrapolate from observational data to our best estimate of the seasonal and annual *C* fluxes. We used shipboard data to calculate the ratios of primary production to gross, net, new and export for any given station, and then these ratios were used to derive *C* uptake

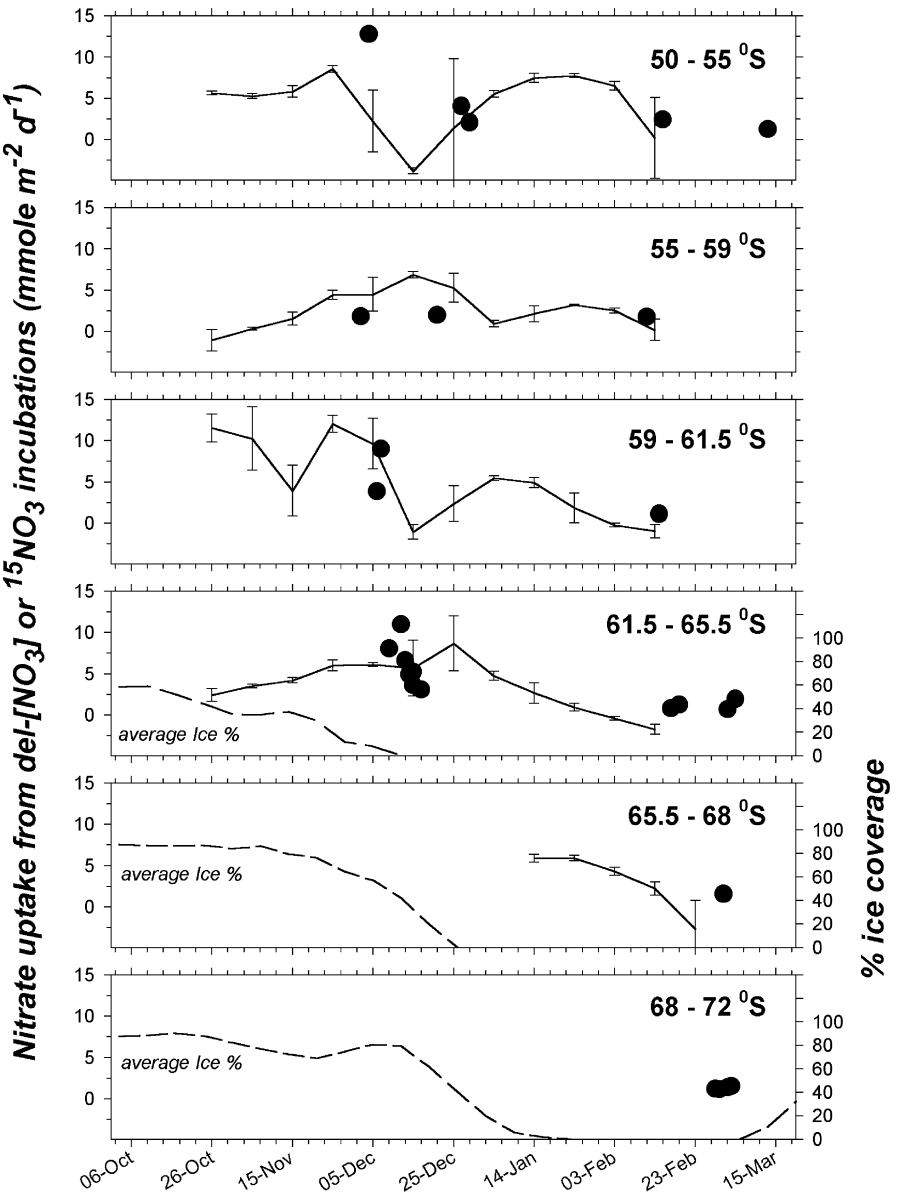

Fig. 5. Plots of the local change in surface nitrate concentration and instantaneous $^{15}NO_3$ uptake rates (mmol m^{-2} d^{-1}; left *Y*-axis) vs. time binned by latitudinal bands as indicated. Ship-based measurements of $^{15}NO_3$ uptake are shown as solid circles. Regional nitrate budgets were used to calculate the local rate of change (see text for details) which is shown as a weekly average by the solid line, with the standard deviation shown by the vertical bar. Dashed line represents mean ice coverage as in Fig. 3.

and export rates from the model-derived primary production cycle. Using this approach, average daily values for the October–May period are plotted (Fig. 6) and tabulated as the seasonal and annual averages (Table 3).

With these extrapolated data sets, we now have the ability to examine the relative rates of production and export for an entire growth cycle across the major Southern Ocean ecological provinces. We find that gross production decreases

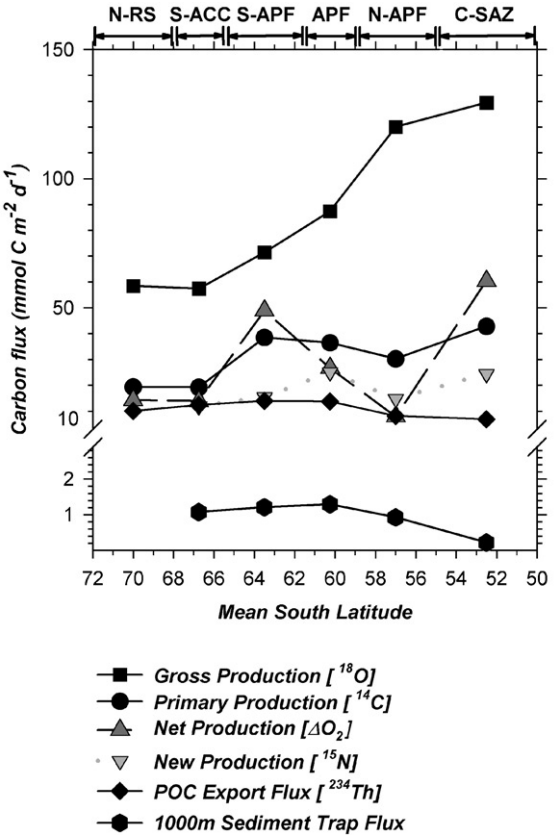

Fig. 6. Plot of gross, primary, net, and new production, POC export at 100 and the 1000 m sediment trap POC flux vs. latitude. Data are all plotted in units of mmol $C\,m^{-2}\,d^{-1}$ averaged for the growing season October–May, and are binned by latitude as indicated along the upper *X*-axis.

steadily from a daily average of 130 to near 60 mmol $C\,m^{-2}\,d^{-1}$ in waters south of 65.5°S (Fig. 6). Net, primary and new production are all highest at the northernmost band in the SAZ, but the southward gradient is not as steep. These rates drop slightly (for new and primary production) or sharply (for net production) between the SAZ and the Polar Frontal regions where there are generally lower chlorophyll levels throughout the growing season. Ratios of new to primary production are quite high in these latitudes, ranging from 40% to 70% as an average during the growing season.

Net to gross production ratios provide information on how efficiently an ecosystem retains production as biomass (Bender et al., 1999). Seasonally averaged net to gross daily production ratios are 0.08 and 0.46 north of 60°S, compared to 0.30 in the APF and 0.25–0.64 south of the APF. The high percentage of production retained in the MIZ of the S-APF is similar to values reported for phytoplankton blooms in other sectors of the Southern Ocean (Williams, 1998). In contrast, the extremely low net to gross production ratio (8%) just north of the APF suggests that intense recycling of biogenic carbon characterize this latitudinal band throughout the growing season.

For POC export, the latitudinal and seasonal fluxes are significantly different, with peak seasonal or annual fluxes being associated with the APF or S-APF and lower both north and south of this region (Table 3). 60–110% of the new production can be balanced by export at all latitudes except the northernmost one (C-SAZ). While we do not have deep trap fluxes further south than 67°S, these trap data also show generally lower POC export in the subantarctic front, despite the higher chlorophyll and production rates at these more northerly latitudes (Fig. 6; Honjo et al., 2000). The POC flux/primary production rate for the season in the SAZ (16%; Table 3) is still relatively high compared to most open ocean settings (Buesseler, 1998). What is unique here are the exceptionally high rates of export at lower productivity rates further south (POC flux/primary production = 33–64%). This extremely high export ratio has been commented on earlier by Buesseler et al. (2001) and is one of the characteristic features of the Southern Ocean in general and these MIZs in particular along 170°W.

It has been suggested that the unusually high efficiency of shallow POC export is related to the planktonic community structure, which forms an efficient pathway for POC and associated bioelement removal at the end of the diatom and *Phaeocyctis* blooms (see further discussion below). Since we are comparing the relative rates of export and production over seasonal time scales, our observation of high export ratio is relevant to the entire growing period, and suggests a very efficient biological pump for this entire region, and for the southernmost stations in particular.

Laws et al. (2000) developed ecological arguments to simplify the estimate of the variable ratio of export to total production. This approach used both temperature and primary production to predict a hyperbolic relationship between "ef" and primary production ("ef" = the ratio of either new production/primary production or export production/primary production, i.e. our export ratio). Although the data for calibrating this relationship was limited in the Southern Ocean to regions of the Ross and Weddell Seas, they note that colder regions have generally higher export efficiency, and that temperature alone accounts for 86% of the variance in "ef" (Fig. 4 in Laws et al., 2000).

When treated in the same manner, our data also show a linear relationship between export/production and temperature although the current data suggest significantly lower export ratios at a given temperature than does the Laws et al. (2000) relationship. A full analysis of how the export ratio in the ACC region differs from that in the more coastal region of the Southern Ocean is beyond the scope of this paper. However, we suggest that the difference here is in the application of more robust estimates for export and production for the Southern Ocean region along 170°W in particular, and in the co-varying factors, such as diatom community structure and Si and Fe limitation (see below) that are responsible for the slope of this export/production vs. temperature relationship, factors that were not included in the original Laws et al. (2000) analysis. This suggests that caution be used when applying simple export/production relationships to larger satellite-derived productivity data sets to determine global C flux or for predicting future change.

4.4. Timing of export vs. production

While only limited ship-based observations of production and export are available for any given latitudinal band over the entire season, we contend that we have captured the major growth and export cycles by utilizing remotely sensed chlorophyll data. Temporal offsets in production and export are large for any given latitude and cruise, thus at single points during the year, the ratio of POC flux to primary production would be highly variable. For example, by the time of Cruise 4, the 170°W transect exhibited extremely low rates of gross, new, and primary production (Fig. 1c, e and f) and even negative rates of net production consistent with the senescence of a prior algal bloom (Table 2). The high POC flux seen at 70–72°S around March 15 occurs much later than the peak chlorophyll seen at the same latitude 1 month earlier in mid-February (chlorophyll peak estimated from satellite data; also compare Fig. 1c and d). Similarly, the peak POC fluxes seen at 65°S around February 1, are observed about 1 month after the peak in chlorophyll levels and new production in the MIZ at this same latitude. This lag between new production and export is similar to that observed between the onset of elevated new production due to the southwest monsoon and particle flux in the northern Arabian Sea (Sambrotto, 2001). Since the ^{234}Th tracer used to derive POC flux has a 24 d half live, fluxes derived from ^{234}Th reflect POC export on time scales of days to weeks prior to the arrival at any given station. Without Lagrangian time-series data on both production and export, it is hard to pinpoint the offset in time any better between the start of the MIZ bloom and its demise, however that time scale must be 1 month or less, based on the export data and changes in chlorophyll stocks measured by the satellite discussed here. A similar conclusion was reached at the APF based upon bio-optical moorings deployed during AESOPS (Abbott et al., 2000).

4.5. Phytoplankton community structure and C fluxes

The seasonal progression of C uptake and export in the AESOPS region is related to the observed changes in the phytoplankton community structure. There were three characteristic planktonic communities along 170°W as determined by microscopic and flow cytometric analyses (Landry et al., 2002; Brown and Landry, 2001; Selph et al., 2001). Northern stations (C-SAZ; N-APF) where Si levels were relatively low throughout the year, were dominated by small prymnesiophyte autotrophs and dinoflagellate

heterotrophs, and in these communities nutrients and carbon would be efficiently recycled in the water column. This corresponds to our region of low POC flux in general (Fig. 1c) and lower export:production ratios throughout the entire growing season (Table 3).

The second major region is within the APF and S-APF, i.e. a zone within which the Si front was seen to migrate from 61°S to 65°S as the season progressed. These stations exhibited some of the highest production and chlorophyll levels in the MIZ. Here, Landry et al. (2002) saw a predominance of large centric and large pennate diatoms early in the season that were not efficiently grazed by the zooplankton community. The high fucoxanthin levels found during December through January are also supportive of high diatom biomass in this region (Fig. 1h). Brzezinski et al. (2001) estimated that the seasonal displacement of the Si gradient can be accounted for by diatom consumption and export. Incubation studies suggest that Fe limited Si uptake early in the season, but after the massive Si drawdown, uptake of Si became substrate limited (Franck et al., 2000). Peak abundances of these larger diatom-dominated communities set the stage for high export of POC and bSi export within 1 month after the peak in biomass, and the maximum ratio of bSi:POC is seen in the 100 and 1000 m particle flux data from this region (Buesseler et al., 2001). Surface Fe levels at these latitudes drop from >0.2 to <0.2 nmol between December and January as the season progresses (Measures and Vink, 2001). One would expect efficient export of phtyoaggregates in response to low Fe which has been suggested to increase sinking rates of diatoms in general (Muggli et al., 1996; Waite and Nodder, 2001).

Later on during the summer in the APF and S-APF, the large diatom-dominated community is replaced with a smaller pennate diatom and non-diatom species (Landry et al., 2002) which are more efficient at recycling C and associated nutrients (Dickson and Orchardo, 2001) and may be more efficient at iron uptake (see below). During this period, biomass and productivity levels decline by the time of cruise 3 in January, and both export and productivity are low during cruise 4 in February at these latitudes.

The third distinct biogeochemical community is found south of 65.5°S, where we find in the MIZ high-chlorophyll levels using satellite data. At these more southerly stations, we also measured some of the highest POC fluxes (Fig. 1d). A different community of slender pennate diatoms and *Phaeocyctis* dominated the phytoplankton community in these continuously high-Si waters, however, our interpretation of the seasonal dynamics at these southernmost latitudes is limited as we have no cruise data early in the growing season. On a seasonal or annual basis, productivity is lower here than further north near the APF, but the export ratio for POC south of 65.5°S is the highest for the entire region (POC flux/primary production $>50\%$). These southernmost plankton communities are thus characterized by a short growing season, high ice-edge chlorophyll concentrations, and efficient POC export. This is similar to data from the Ross Sea proper, where ^{234}Th-derived export and changes in POC stocks indicated that 30–50% of the POC derived from the phytoplankton blooms is exported below the euphotic zone (Smith et al., 2000; Cochran et al., 2000).

4.6. Controls on production and export iron and silica limitation

Controls on production and export in the SIZ are tied to changes in community structure, which in this HNLC region, appear to be associated with shifts in Fe and Si limitation. The photosynthetic parameter F_v/F_m can be useful indicators of Fe stress. F_v/F_m, the ratio of variable fluorescence to maximal fluorescence, is a quantitative measure of the quantum efficiency of plankton photosystem II (e.g. Kolber et al., 1994). Values of F_v/F_m lower than the theoretical maximum of 0.65 have been used as an indicator of Fe stress. This parameter was measured here on cruise 4 by Sosik and Olsen (2002) and showed a trend from values >0.4 in the upper 40 m at the APF and northward, decreasing to values around 0.25–0.30 south of 65°S. These investigators saw a positive correlation between F_v/F_m and ambient Fe concentrations (determined by the FIA technique, Measures and Vink, 2001) and a negative correlation with mean cell diameter.

Thus on cruise 4, the waters south of 65°S which have the lowest Fe levels also have the lowest F_v/F_m indicative of Fe stress and larger mean cell size (3–4 μm mean cell diameter vs. 1 μm north of the APF; Sosik and Olson, 2002).

Within Cruise 4, there is a correlation of increasing POC export with decreasing F_v/F_m (Fig. 7). This is the first time this has been documented for a given region; however, time series data during iron enrichment experiments have shown that an initial increase of F_v/F_m associated with reduced Fe stress can be followed by a decrease in F_v/F_m associated with the export of diatoms as they sink out of an Fe fertilized patch (Bidigare et al. 1999). This association of higher F_v/F_m with low flux and low F_v/F_m with high flux may reflect the predominance of small cells in the northern stations which are established after the bloom of large diatoms, and result in low export, vs. the more recently ice free southern sites which are likely always Fe poor but still regions of enhanced POC export.

For further evidence of Fe controls on production and export earlier in the growing season, we can use the photosynthetic parameter P^B_{opt}, which is the highest chlorophyll-normalized productivity rate determined in on-deck incubations. P^B_{opt} and F_v/F_m are positively correlated with each other during cruise 4 (Hiscock et al., 2003), and both showed lower values at the southernmost stations south of 65.5°S, indicative of Fe stress. At the APF and S-APF, P^B_{opt} increases between Cruises 1 and 2 from 2.5 ± 0.8 to 4.7 ± 1.1, as increased stratification and sufficient Fe levels lead to the onset of the bloom of large diatoms (P^B_{opt} data in units of mg C mg Chl^{-1} h^{-1}). High-frequency bio-optical measurements at the APF from moorings suggest that the buildup to maximum chlorophyll levels takes on the order of 2–3 weeks, similar to what is seen in the satellite data (Abbott et al., 2000). As the season progressed, the community shifted from the larger diatoms to smaller species with lower Si and presumably lower Fe requirements as indicated by P^B_{opt} (and F_v/F_m), which remained elevated through cruise 4 at these latitudes (mean $=4.7\pm1.0$ from 59°S to 65.5°S). South of 65.5°S, we only have P^B_{opt} data during cruise 4, when P^B_{opt} was significantly lower (2.6 ± 0.7) indicative of Fe stress, similar to the trend in F_v/F_m.

If Fe is the control on the ability to form blooms of large diatoms in the APF and S-APF regions, it is interesting that P^B_{opt} and F_v/F_m remain relatively high near the APF and S-APF during cruise 4,

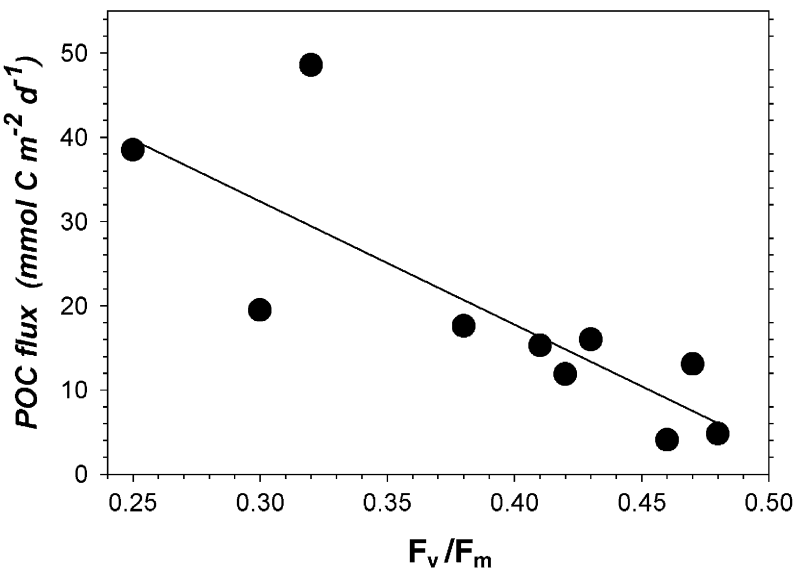

Fig. 7. Plot of POC flux at 100 m (mmol C m^{-2} d^{-1}; *Y*-axis) vs. F_v/F_m (average for upper 40 m from Sosik and Olsen (2002) for stations sampled during Cruise 4. Solid line is linear regression through data ($r^2 = 0.66$).

despite a decrease in ambient Fe and extremely low rates of production. One explanation is that there is a community shift to smaller species, more adapted to low ambient Fe. In contrast, the waters south of 65.5°S may never have been high enough in Fe to support the growth of large diatoms. By the time of Cruise 4, the lowest ratios of F_v/F_m and P^B_{opt} were observed in these southernmost stations where the lowest Fe levels were found. What is unclear is whether or not the blooms in the southernmost stations are initiated by an increase in Fe released from melting ice. In this case, one might expect increased F_v/F_m or P^B_{opt} early in the season, and on Cruise 3, we did see the high fucoxanthin pigment levels between 65°S and 68°S. Unfortunately, we have no cruise-based production data south of 65.5°S during the early ice melt period when the satellite observations show peak chlorophyll levels.

5. Summary and conclusions

The AESOPS study along 170°W provides one of the most complete seasonal data sets on production and export in the Subantarctic, Polar Frontal and SIZs of the Southern Ocean. Concurrent satellite data allow us to extend our analyses to periods when shipboard observations were not available. The combined data suggest that the dominant feature with respect to plankton biomass, is the association of high chlorophyll levels with the retreat of the sea ice which begins in October just south of the Polar Front. These biomass peaks move further south between December and February as the sea ice retreats. Export lags production by up to 1 month, with the highest export ratio being associated with the MIZ south of 65.5°S.

A productivity model taking advantage of measured P^B_{opt} values and satellite chlorophyll data, indicates that prior model-based estimates of primary production rates in this region were low. We see primary production rates as high as 150 mol C m^{-2} d^{-1}just south of the Polar Front. With this model, we can more accurately extrapolate to an annual production rate of 10 mol C m^{-2} yr^{-1} in the PFZ to 65.5°S, 4 mol C m^{-2} yr^{-1} between 65.5°S and 72°S and 9–13 mol C m^{-2} yr^{-1} in the region north of the APF in the SAZ. These rate are 50% or more higher than other model-based or measured rates of production in the APF, and up to two or more times greater than other estimates in the SIZ (Wefer and Fischer, 1991; Tréguer and Jacques, 1992; Quéguiner et al., 1997; Moore and Abbott, 2000). These higher rates are due both to our improved primary productivity model, and the fact that the SIZ in this sector of the Southern Ocean is characterized by higher than average chlorophyll levels (Moore and Abbott, 2000).

The onset of the blooms throughout this region is initiated by shoaling of the mixed layer in the spring, either due to warming alone, or the presence of low salinity melt waters in the SIZ. Subsequent shifts in community structure associated with ambient Fe and Si levels appear to control the relative rates of C uptake and export. From an analysis of these factors, we can broadly divide the AESOPS transect into three distinct biogeochemical communities. One community found at stations north of the Polar Front between 50°S and 59°S, is characterized by relatively low Si and NO_3, with slightly higher daily primary production rates associated with early and late season chlorophyll maxima. The export ratio (= POC flux at 100 m/primary production) associated with a community of small autotrophic and heterotrophic plankton at these latitudes falls between 16% and 26% which is low relative to the regions further south, but still high relative to most other ocean settings.

At the APF and S-APF, defined here as latitudes between 59°S and 65.5°S, we see a second community characterized by large diatoms which bloom in association with the onset of stratification during the spring. Export efficiencies in this region are 33–38% on a seasonal basis. Other AESOPS studies suggest that the seasonal drawdown of Si in this region and export of POC and bSi is driven by this spring bloom of large diatoms. With the termination of this large diatom bloom, a pennate diatom and non-diatom community emerges which would appear to be adapted to lower Fe levels as indicated by F_v/F_m and P^B_{opt} data, however, production and export

remain low throughout the remainder of the growing season.

South of 65.5°S, we see the highest export efficiencies (> 50%) in a third type of phytoplankton community that is presumably always Fe stressed and where we do not see evidence of large diatoms or associated Si drawdown. The MIZ in this region is characterized by high chlorophyll levels, a short growing season and an efficient biological pump. The AESOPS cruises did not sample this region during the early bloom stages, thus the impact of melting ice on relieving Fe stress and the seasonal dynamics in community structure cannot be assessed. This region has similarities to the Ross Sea proper, or more specifically the northern stations sampled earlier during AESOPS and other studies (Smith and Nelson, 1986; Smith et al., 2000; Cochran et al., 2000).

These large shifts in the production and export balance with time and space, make comparisons with single cruises in different Southern Ocean studies difficult. Common physical and chemical conditions, such as ice cover, light, mixed-layer depth, macro- and minor nutrient levels, are all important factors in controlling the ecosystem structure that drives the rates of C uptake and export in the Southern Ocean. This combination of high-quality seasonal field studies and satellite observations is a major contribution of AESOPS to our further understanding of the Southern Ocean C cycle.

Acknowledgements

We are pleased to thank the crews of the R/V *Roger Revelle,* our collaborators on board, and the overall efforts of Robert Anderson and Walker Smith in leading the AESOPS program. In addition, many people assisted us either at sea, during analyses and in the interpretation of these results, including: M.P. Bacon, J.K. Cochran, H. Sosik, R. Olson, M. Landry and J. Marra. The manuscript also benefited from three anonymous reviews. Funding was obtained under US National Science Foundation grants OPP-9530861 to KOB; OPP-9531981 to RTB; OPP-9530746 to M. Bender and MLD and OCE-9819151 to RNS. MRH was supported by a graduate fellowship from the American Meteorological Society and NASA's "Mission to Planet Earth" program. The authors would also like to thank the SeaWiFS project (Code 970.2) and the Distributed Active Archive Center (Code 902) at the Goddard Space Flight Center, Greenbelt, MD 20771, for the production and distribution of the ocean color data, respectively. These activities are sponsored by NASA's Earth Science Enterprise Program. We would also like to thank the NOAA/NASA Pathfinder Project for the satellite SST data used in this work and the National Snow and Ice Data. This is WHOI contribution # 10723, LDEO contribution #6338 and JGOFS contribution #802

References

Abbott, M.R., Richman, J.G., Letelier, R.M., Bartlett, J.S., 2000. The spring bloom in the Antarctic Polar Frontal Zone as observed from a mesoscale array of bio-optical sensors. Deep-Sea Research II 47 (15-16), 3285–3314.

Barth, J.A., Cowles, T.J., Pierce, S.D., 2001. Mesoscale physical and bio-optical structure of the Antarctic Polar Front near 170°W during austral spring. Journal of Geophysical Research 106 (C7), 13879–13902.

Behrenfeld, M.J., Falkowski, P.G., 1997. Photosynthetic rates derived from satellite-based chlorophyll concentration. Limnology and Oceanography 42, 1–20.

Bender, M., Grande, K., Johnson, K., Marra, J., Williams, P.J.leB., Sieburth, J., Pilson, M., Langdon, C., Hitchcock, G., Heinemann, C., 1987. A comparison of four methods for the determination of planktonic community metabolism. Limnology and Oceanography 32, 1085–1098.

Bender, M., Orchardo, J., Dickson, M.-L., Barber, R., Lindley, S., 1999. In vitro O_2 fluxes compared with ^{14}C production and other rate terms during the JGOFS Equatorial Pacific experiment. Deep-Sea Research I 46, 637–654.

Bidigare, R.R., Hanson, K.L., Buesseler, K.O., Wakeham, S.G., Freeman, K.H., Pancost, R.D., Millero, F.J., Steinberg, P., Popp, B.N., Latasa, M., Landry, M.R., Laws, E.A., 1999. Iron-stimulated changes in ^{13}C fractionation and export by equatorial Pacific phytoplankton. Paleoceanography 14 (5), 589–595.

Brown, S.L., Landry, M.R., 2001. Microbial community structure and biomass in surface waters during a Polar Front summer bloom along 170°W. Journal of Geophysical Research 106 (C7), 13917–13930.

Brzezinski, M.A., Nelson, D.M., Franck, V.M., Sigmon, D.E., 2001. Silicon dynamics within an intense open-ocean diatom bloom in the Pacific sector of the Southern Ocean. Deep-Sea Research II 48 (19-20), 3997–4018.

Buesseler, K.O., 1998. The de-coupling of production and particulate export in the surface ocean. Global Biogeochemical Cycles 12 (2), 297–310.

Buesseler, K.O., Bacon, M.P., Cochran, J.K., Livingston, H.D., 1992. Carbon and nitrogen export during the JGOFS North Atlantic Bloom Experiment estimated from ^{234}Th:^{238}U disequilibria. Deep-Sea Research I 39 (7/8), 1115–1137.

Buesseler, K.O., Ball, L., Andrews, J., Cochran, J.K., Hirschberg, D.J., Bacon, M.P., Fleer, A., Brzezinski, M., 2001. Upper ocean export of particulate organic carbon and biogenic silica in the Southern Ocean along 170°W. Deep-Sea Research II 48 (19-20), 4275–4297.

Cochran, J.K., Buesseler, K.O., Bacon, M.P., Wang, H.W., Hirschberg, D.J., Ball, L., Andrews, J., Crossin, G., Fleer, A., 2000. Short-lived thorium isotopes (^{234}Th, ^{228}Th) as indicators of POC export and particle cycling in the Ross Sea, Southern Ocean. Deep-Sea Research II 47 (15-16), 3451–3490.

DeMaster, D.J., Nelson, T.M., Harden, S.L., Nittrouer, C.A., 1991. The cycling and accumulation of biogenic silica and organic carbon in Antarctic deep-sea and continental margins. Marine Chemistry 35, 489–502.

Dickson, M.-L., Orchardo, J., 2001. Oxygen production and respiration in the Antarctic Polar Front region during the austral spring and summer. Deep-Sea Research II 48 (19-20), 4101–4126.

Franck, V.M., Brzezinski, M.A., Coale, K.H., Nelson, D.M., 2000. Iron and silicic acid concentrations regulate Si uptake north and south of the Polar Frontal Zone in the Pacific Sector of the Southern Ocean. Deep-Sea Research II 47 (15-16), 33145–33338.

Gaarder, T., Gran, H., 1927. Investigations of the production of plankton in the Oslo Fjord. Rapport et Proces-Verbaux des Reunions, Conseil International pour l'Exploration de la Mer 42, 1–48.

Gregg, W.W., Carder, K.L., 1990. A simple spectral solar irradiance model for cloudless maritime atmospheres. Limnology and Oceanography 35, 1657–1675.

Griffiths, F.B., Bates, T.S., Quinn, P.K., Clementson, L.A., Parslow, J.S., 1999. The oceanographic context of the first aerosol characterization experiment (ACE 1): a physical, chemical, and biological overview. Journal of Geophysical Research 104, 21649–21671.

Hiscock, M.R., Marra, J., Smith, W.O., Goericke, R., Measures, C.I., Vink, S., Olson, R.J., Sosik, H.M., Barber, R.T., 2003. Primary productivity and its regulation in the Pacific Sector of the Southern Ocean. Deep Sea Research Part II, this issue (doi: 10.1016/S0967-0645(02)00583-0).

Honjo, S., Francois, R., Manganini, S., Dymond, J., Collier, R., 2000. Export fluxes in the western Pacific sector of the Southern Ocean along 170°W. Deep-Sea Research II 47 (15-16), 3521–3548.

Joos, F., Siegenthaler, U., 1991. Possible effects of iron fertilization in the Southern Ocean on atmospheric CO_2 concentration. Global Biogeochemical Cycles 5, 135–150.

Kolber, Z.S., Barber, R.T., Coale, K.H., Fitzwater, S.E., Greene, R.M., Johnson, K.S., Lindley, S., Falkowsky, F.G., 1994. Iron limitation of phytoplankton photosynthesis in the equatorial Pacific Ocean. Nature 371, 145–149.

Kopczynska, E., Dehairs, F., Elskens, M., Wright, S., 2001. Phytoplankton and microzooplankton variability between the Subtropical and Polar Fronts south of Australia: thriving under regenerative and new production in late summer. Journal of Geophysical Research 106 (C12), 31597–31609.

Landry, M.R., Selph, K.E., Brown, S.L., Abbott, M.A., Measures, C.I., Vink, S., Allen, C.B., Calbet, A., Christensen, S., Nolla, H., 2002. Seasonal dynamics of phytoplankton in the Antarctic Polar Front region at 170°W. Deep-Sea Research II 49 (9-10), 1843–1865.

Laws, E.A., 1991. Photosynthetic quotients, new production, net community production in the open ocean. Deep-Sea Research I 38, 143–167.

Laws, E.A., Falkowski, P.G., Smith Jr., W.O., Ducklow, H., McCarthy, J.J., 2000. Temperature effects on export production in the open ocean. Global Biogeochemical Cycles 14 (4), 1231–1246.

Lewis, M.R., Smith, J.C., 1983. A small volume, short-incubation-time method for measurement of photosynthesis as a function of incident irradiance. Marine Ecology Progress Series 13, 99–102.

Measures, C.I., Vink, S., 2001. Dissolved Fe in the upper waters of the Pacific Sector of the Southern Ocean. Deep-Sea Research II 48 (19-20), 3913–3941.

Moore, J.K., Abbott, M.R., 2000. Phytoplankton chlorophyll distributions and primary production in the Southern Ocean. Journal of Geophysical Research 105, 28709–28722.

Moore, J.K., Abbott, M.R., Richman, J.G., Smith, W.O., Cowles, T.J., Coale, K.H., Gardner, W.D., Barber, R.T., 1999. SeaWiFS satellite ocean color data from the Southern Ocean. Geophysical Research Letters 26, 1465–1468.

Morel, A., 1988. Optical modeling of the upper ocean in relation to its biogenous matter content (Case I waters). Journal of Geophysical Research 93, 10749–10768.

Morrison, J.M., Gaurin, S., Codispoti, L.A., Takahashi, T., Millero, F.J., Gardner, W.D., Richardson, M.J., 2001. Seasonal evolution of hydrographic properties in the Antarctic Circumpolar Current at 170°W during 1997–1998. Deep-Sea Research II 48 (19-20), 3943–3972.

Muggli, D.L., Lecourt, M., Harrison, P.J., 1996. Effects of iron and nitrogen source on the sinking rate, physiology and metal composition of an oceanic diatom from the subarctic Pacific. Marine Ecological Progress Series 132, 215–227.

Nelson, D.M., DeMaster, D.J., Dunbar, R.B., Smith Jr., W.O., 1996. Cycling of organic carbon and biogenic silica in the Southern Ocean: estimates of water-column and sedimentary fluxes on the Ross Sea continental shelf. Journal of Geophysical Research 101, 18519–18532.

Nelson, D.M, Anderson, R.F., Barber, R.T., Brzezinski, M.A., Buesseler, K.O., Chase, Z., Collier, R.W., Dickson, M.L., Francois, R., Hiscock, M.R., Honjo, S., Marra, J., Martin, W.R., Sambrotto, N., Sayles, F., Sigmon, D.E., 2002. Vertical budgets for organic carbon and biogenic silica in

the Pacific sector of the Southern Ocean, 1996-1998. Deep-Sea Research II 49, 1645–1674.

Pondaven, P., Ragueneau, O., Tréguer, P., Hauvespre, A., Dezileau, L., Reyss, J.L., 2000. Resolving the 'opal paradox' in the Southern Ocean. Nature 405, 168–172.

Quéguiner, B., Tréguer, P., Peeken, I., Scharek, R., 1997. Biogeochemical dynamics and the silicon cycle in the Atlantic sector of the Southern Ocean during austral spring 1992. Deep-Sea Research II 44, 69–89.

Sambrotto, R.N., 2001. Nitrogen production in the northern Arabian Sea during the Spring Intermonsoon and Southwest Monsoon seasons. Deep-Sea Research II 48 (6-7), 1173–1198.

Sambrotto, R.N., Mace, B.J., 2000. Coupling of biological and physical regimes across Antarctic Polar Front as reflected by nitrogen production and recycling. Deep-Sea Research II 47 (15-16), 3339–3368.

Sarmiento, J.L., Le Quéré, C., 1996. Oceanic carbon dioxide uptake in a model of century-scale global warming. Science 274, 1346–1350.

Sarmiento, J.L., Orr, J.C., 1991. Three-dimensional simulations of the impact of Southern Ocean nutrient depletion on atmospheric CO_2 and ocean chemistry. Limnology and Oceanography 36, 1928–1950.

Sayles, F.L., Martin, W.R., Chase, Z., Anderson, R.F., 2001. Benthic remineralization and burial of biogenic SiO_2 and $CaCO_3$, organic carbon and detrital material in the Southern Ocean along a transect at 170°West. Deep-Sea Research II 48 (19-20), 4323–4383.

Sedwick, P.N., DiTullio, G.R., 1997. Regulation of algal blooms in Antarctic shelf waters by the release of iron from melting sea ice. Geophysical Research Letters 24, 2515–2518.

Selph, K.E., Landry, M.R., Allen, C.B., Calbet, A., Christensen, S., Bidigare, R.R., 2001. Microbial community composition and growth dynamics in the Antarctic Polar Front and seasonal ice zone during late spring 1997. Deep-Sea Research II 48 (19-20), 4059–4080.

Smith, W.O., Nelson, D.M., 1985. Phytoplankton bloom produced by a receding ice edge in the Ross Sea: spatial coherence with the density field. Science 227, 163–166.

Smith Jr., W.O., Marra, J., Hiscock, M.R., Barber, R.T., 2000. The seasonal cycle of phytoplankton biomass and primary productivity in the Ross Sea, Antarctica. Deep-Sea Research II 47, 3119–3140.

Sosik, H.M., Olson, R.J., 2002. Phytoplankton and iron limitation of photosynthetic efficiency in the Southern Ocean during late summer. Deep-Sea Research I 49 (7), 1195–1216.

Tréguer, P., Jacques, G., 1992. Dynamics of nutrients and phytoplankton, and fluxes of carbon, nitrogen and silicon in the Antarctic Ocean. Polar Biology 12, 149–162.

Waite, A.M., Nodder, S.D., 2001. The effect of in situ iron addition on the sinking rates and export flux of Southern Ocean diatoms. Deep-Sea Research II 48, 2635–2654.

Wefer, G., Fischer, G., 1991. Annual primary production and export flux in the Southern Ocean from sediment trap data. Marine Chemistry 35, 597–613.

Williams, P.J.leB., 1998. The balance of plankton respiration and photosynthesis in the open ocean. Nature 394, 55–57.